PAPER

Room temperature single photon source using fiber-integrated hexagonal boron nitride

To cite this article: Tobias Vogl *et al* 2017 *J. Phys. D: Appl. Phys.* **50** 295101

View the article online for updates and enhancements.

Room temperature single photon source using fiber-integrated hexagonal boron nitride

Tobias Vogl[1], Yuerui Lu[2] and Ping Koy Lam[1]

[1] Centre for Quantum Computation and Communication Technology, Department of Quantum Science, Research School of Physics and Engineering, The Australian National University, Acton ACT 2601, Australia
[2] Research School of Engineering, The Australian National University, Acton ACT 2601, Australia

E-mail: Tobias.Vogl@anu.edu.au and Ping.Lam@anu.edu.au

CrossMark

Abstract

Single photons are a key resource for quantum optics and optical quantum information processing. The integration of scalable room temperature quantum emitters into photonic circuits remains to be a technical challenge. Here we utilize a defect center in hexagonal boron nitride (hBN) attached by Van der Waals force onto a multimode fiber as a single photon source. We perform an optical characterization of the source in terms of spectrum, state lifetime, power saturation and photostability. A special feature of our source is that it allows for easy switching between fiber-coupled and free space single photon generation modes. In order to prove the quantum nature of the emission we measure the second-order correlation function $g^{(2)}(\tau)$. For both fiber-coupled and free space emission, the $g^{(2)}(\tau)$ dips below 0.5 indicating operation in the single photon regime. The results so far demonstrate the feasibility of 2D material single photon sources for scalable photonic quantum information processing.

Keywords: hBN, 2D materials, single photons, integrated photonics

(Some figures may appear in colour only in the online journal)

1. Introduction

The field of two-dimensional (2D) materials has gained much interest during the past few years [1, 2]. Due to their excellent electronic and optical properties, 2D materials offer significant potentials for both industrial technologies and scientific studies. Although most research on 2D materials is targeting Graphene [3, 4] due to its high tensile strength and electrical properties, such as an intrinsic record high electron mobility, the material's application to optics is limited due to the lack of a band gap. It was recently discovered that monolayer transition metal dichalcogenides (TMDs) can host quantum emitters at cryogenic temperatures [5–9]. The defect alters the electronic crystal structure or, more precisely, introduces sub-states within the band gap that typically lie close to the valence or conduction band. For materials with a large band gap, transition levels with greater energy differences to the

bands can occur. This in turn allows defect emission to be distinct from photoluminescence (PL) emission at room temperature as demonstrated in the insulating 2D material hexagonal boron nitride (hBN) [10].

In spite of the pivotal role single photon sources (SPSs) play in many quantum information processing and quantum communication applications [11–13], and the huge efforts made in order to investigate different types of SPSs, building an *ideal* single photon source remains challenging. Among the desired properties of a single photon source are (I) a vanishing second-order correlation function $g^{(2)}(\tau = 0) \rightarrow 0$, (II) a high indistinguishability of the emitted photons, (III) spectral control of the emission (meaning a narrow linewidth and tuning of the center wavelength), (IV) a high brightness and (V) a high coupling efficiency, while (VI) still being able to integrate the source into various environments. Progress has been made on several different types of single photon sources: in SPSs

based on heralded spontaneous parametric down-conversion it was possible to achieve simultaneously outstanding results for most of (I)–(V) [14–18] at the expense of requiring single photon avalanche diodes (SPADs) for heralding and high power excitation lasers. Recent demonstrations of single photon emission from quantum dots caught up with state-of-the-art results in especially (I) and (II) and also in (IV) and (V) [19–22]. However, quantum dots require cooling to liquid helium temperatures making them infeasible for some of the applications. Another extensively studied direction is NV-centers in diamond and similar systems [23]. In contrast a SPS in a 2D material offers versatile integrability and an intrinsic out-coupling efficiency of unity, while at the same time being cost-effective, easy-to-handle and can operate at room temperature and normal pressure.

Here we report a room temperature single photon source using atomically-thin hBN flakes attached to the end face of a high-NA multimode fiber excited by PL. Our setup allows easy switching between fiber-coupled and free space operation. We demonstrate the quantum nature for both modes and approximate the collection efficiency of the fiber.

2. Experimental results

2.1. Device fabrication

First, few-layer hBN flakes are mechanically exfoliated to gel foil (Gel-Pak WF-40-X4) from bulk crystal (acquired from HQGraphene) using 3M scotch tape, and then optically identified with a microscope. In order to enhance the optical contrast of the hBN flakes the latter is done under red light [24]. Still, due to the zero-crossing of the optical contrast of hBN in the visible spectrum, this sets a limit to the minimally achievable layer thickness (typically 4–5 nm). The thickness is calculated by comparing the optical contrast with atomic force microscopy measurements from a previous experiment. In the following the sample undergoes a series of oxygen plasma and thermal treatments, in order to introduce and activate the color centers [25]. We have tried a variety of different settings and found the best results with a 3-stage process: initially, the flakes are are treated for 1 min at a plasma power of 100 W and an oxygen flow of 300 sccm and then for 10 min at 500 W at 600 sccm oxygen flow. During the third step the sample is baked at 160 °C for 30 min. We found that higher temperatures (with the sample on a Si/SiO$_2$ substrate) yield higher brightnesses, however, the used polymer foil is not suitable for higher temperatures. In an intermediate step after the annealing the flakes are characterized in a micro-photoluminescence system (μPLS) with a DPSS laser at a wavelength of 522 nm continuously exciting the sample in a confocal microscope. As the photon energy is below the band gap of hBN ($E_g > 5$ eV [24]), delocalized excitonic emission is prevented making it possible to address distinct defect centers in a photoluminescence experiment. The flakes are scanned to identify regions with a high PL response as shown in figure 1(a) marked with D1–D3. For each position a full spectrum is recorded. The regions with a high PL intensity are regions where the defect centers are localized. If the flake is found not to host a defect center the plasma

treatment is repeated. In the final fabrication step, appropriate flakes are transferred by dry contact onto the cleaved end of a high-NA multimode fiber with a pure silica core (core diameter $d_{core} = 200\,\mu$m, $NA = 0.5$). To ensure depositing the flake at the center of the fiber core the fiber is illuminated through the back end during the transfer process. It is just as much pressure applied such that the air gap between the fiber and the polymer foil closes by itself. After 4 min the polymer foil is removed and with around 70% probability the flake will be transferred to the fiber. The applied pressure and contact time strongly influence this success probability. However, even after an unsuccessful transfer these steps can be repeated. Using this transfer method, the flakes are attached by Van der Waals force to the fiber. Figure 1(b) shows a microscope image under red light of the transferred flake on the end of the fiber. The magnified part shows a post-processed contrast enhanced image of the area of interest with the approximate positions of D1–D3 marked with arrows. The flake thickness is approximately 5 nm, which corresponds to about 12 atomic layers.

2.2. Characterization

After transferring the flakes onto the fiber, the flakes are fully characterized, with all measurements being carried out at room temperature. Preliminary measurements showed a low background noise originating from the fiber which was traced back to Raman scattering [26]. To eliminate this background the flakes are excited under an angle such that the pump light is not guided anymore. The PL response is checked again in order to confirm that the defect survived the transfer process. The following analysis is limited to the defect marked with D1 in figure 1(a), as this defect showed the highest brightness. It is not clear why some defects show a higher brightness than others, the brightness can vary from defect to defect (and including from flake to flake) by a factor of up to 4.7, while more than 80 different samples have been tested. However, although not reproducible for each individual defect, a bright defect can always be re-created by fabricating and testing more samples. The spectrum of the emission of D1 is shown in figure 1(c). As can be seen the spectrum is rather broad as reported in [10] with the maximum PL intensity peaking at 616 nm. Time-resolved PL (TRPL) with the laser in pulsed mode and a pulse length of 300 fs at a repetition rate of 20.8 MHz reveals an effective state lifetime of $\tau = 1.93$ ns extracted from a fit of a single exponential decay function (see figure 1(d)). The effective state lifetime satisfies

$$\frac{1}{\tau} = \frac{1}{\tau_r} + \frac{1}{\tau_{nr}} \tag{1}$$

with τ_r and τ_{nr} being the radiative and non-radiative decay time. Note that this state lifetime sets a physical limit onto minimal timing jitter and also on the maximal repetition frequency of the source. Although we did not measure the lifetime of every defect we tested, we found that the excited state lifetime as well as spectral shape of the emission can vary from defect to defect. However, there is no correlation between brightness and lifetime or spectrum so far. Future investigations together with theoretical modeling will give more insight into
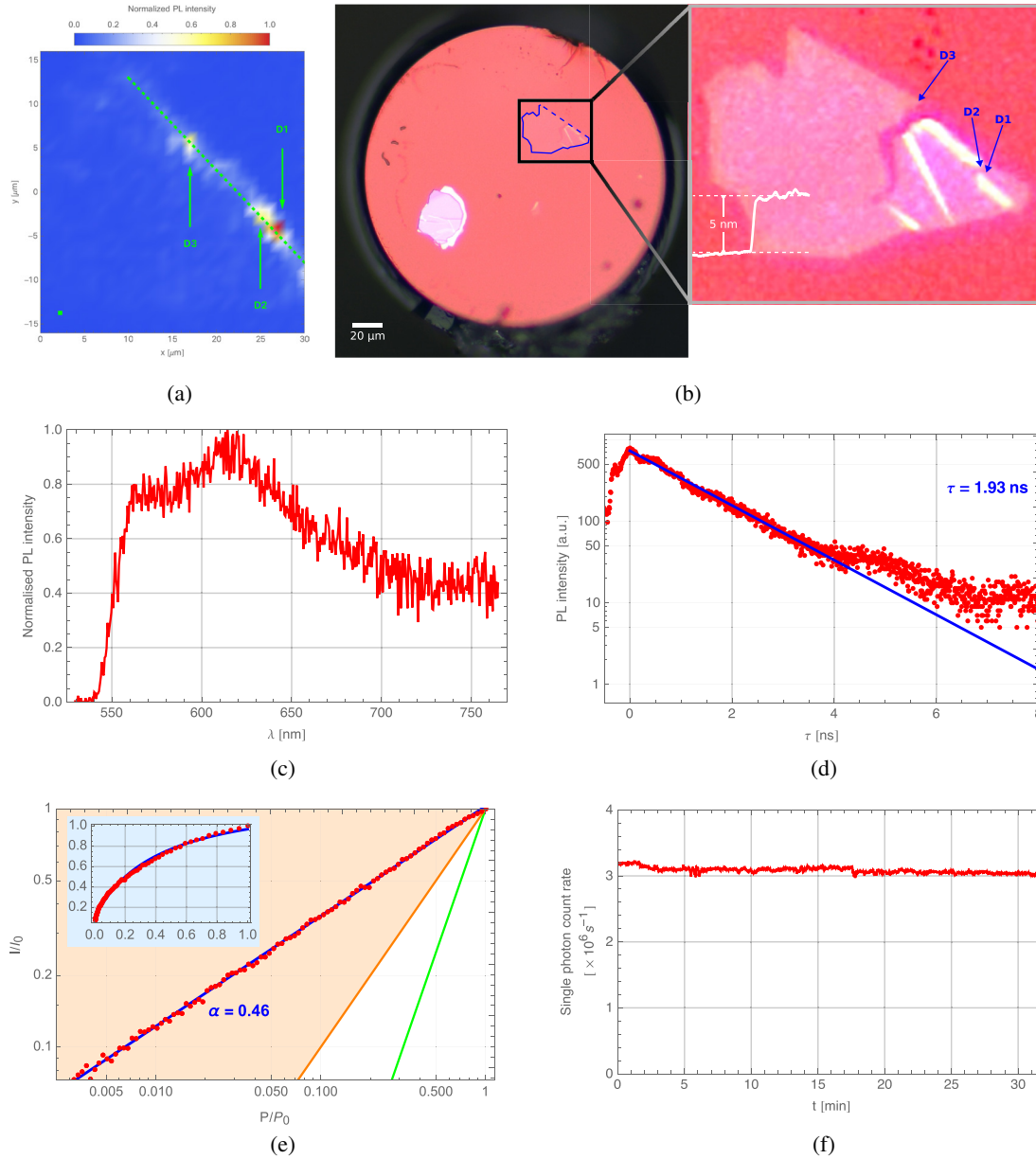
Figure 1. Characterization of the hBN flake on the fiber. (a) μPL scan of the flake revealing the presence of suspected defects labeled D1–D3. The small green box in the bottom left corner indicates the resolution (0.5 μm) of the μPL scan. (b) Optical microscope image of the hBN flake on the fiber under red light with 500 × magnification. The flake is framed in blue with the edge with the defects dashed (see green line in (a)). The top right magnification shows a contrast enhanced image of the flake with the approximate positions D1–D3 marked with arrows and a calculated height profile. (c) Spectrum measured at D1 acquired in-reflection from the flake by excitation with a laser at 522 nm. (d) Time-resolved photoluminescence of D1 reveals an effective decay time of $\tau = 1.93$ ns. (e) Log–Log-plot of the saturation of the PL intensity as a function of laser excitation power. A slope $\alpha < 1$ (orange-shaded area) indicates defect emission, while a slope of $\alpha = 1$ (orange line) would indicate free excitonic emission and a slope of $\alpha = 2$ (green line) bi-excitonic emission. The slope in this measurement ($\alpha = 0.46$) confirms the defect nature of the emission. (f) The single photon count rate as a function of time demonstrates a photostability better $\sigma_{PL}/\overline{R}_{PL} < 1.3\%$. Integration time for each point is 1 s.

the nature of the defect. To find the ideal excitation power a saturation measurement has been done. The PL intensity I as a function of the excitation power P (see figure 1(e), small inset) can be described by

$$I(P) = \frac{I_{sat} \cdot P}{P + P_{sat}} + I_d \tag{2}$$

where I_{sat} and P_{sat} are the saturation intensity and power respectively and I_d is the dark count intensity. From a fit we find the saturation power to be $P_{sat} = 38.2\ \mu$W. With a focused

laser spot size diameter of 0.67 μm this amounts to an intensity of 2.71 kW cm^{-2} which is found to be below the damage threshold for the flakes. We measured the damage threshold by increasing the laser intensity up to 2.18 MW cm^{-2} (average intensity from a pulsed laser with a duty cycle of $6.24 \cdot 10^{-6}$) and exposed the sample for a minute. We note that this is just a lower bound for the damage threshold, as we did not increase the laser power until it actually damaged the sample. However, if the power dependence is plotted on a Log–Log-scale the nature of the emission can be determined:
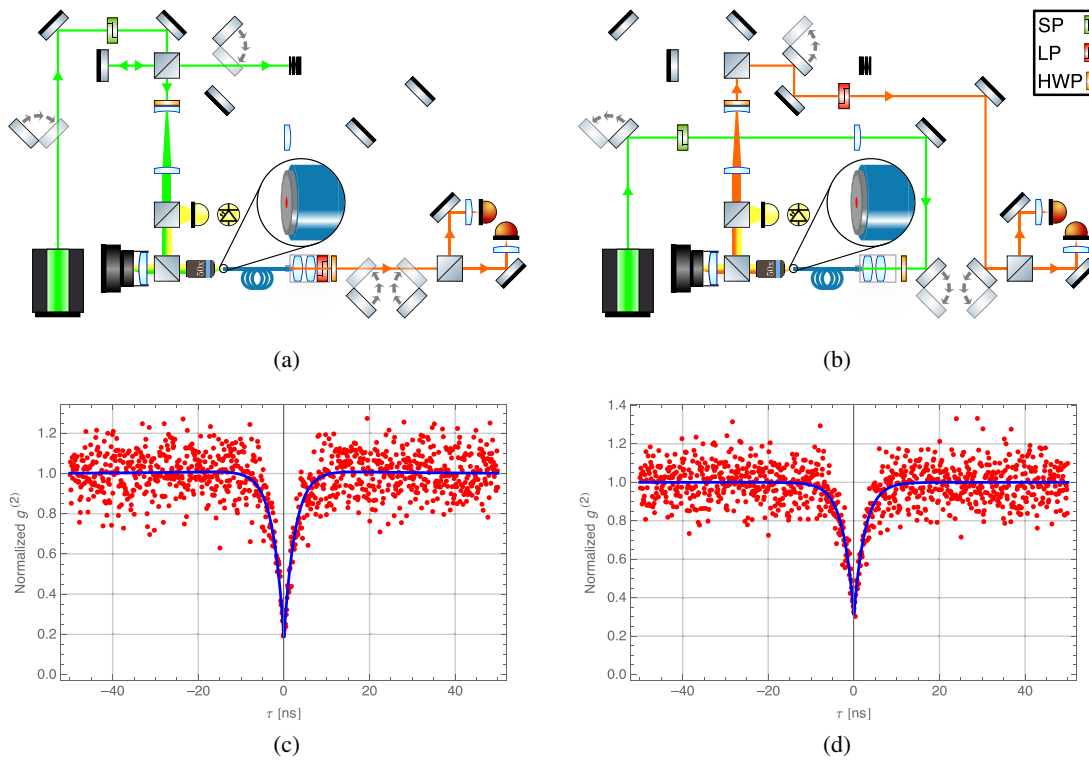
Figure 2. Measurements of the second order correlation function. (a) Setup for operation in fiber-coupled-mode. For easing the coupling of the free space collection the laser is split into reference and pump beam. The pump light is then expanded and coupled into a confocal microscope with the fiber end with the hBN flake loaded at the focal point (small inset, the position of the hBN flake is indicated by a red hexagon). The light is then spectrally filtered and collimated. Finally, the emitted photons are detected in a HBT-type interferometer. (b) Setup for operation in free space-mode. By flipping the four flip mirrors, the defect can be excited via the fiber and the photons can be collected via free space. SP: shortpass filter, LP: longpass filer, HWP: half wave plate. (c) $g^{(2)}(\tau)$ as measured at the fiber output. (d) $g^{(2)}(\tau)$ as measured with free space collection.

the slope $\alpha = 1$ means, the emission originates from a free exciton, a slope close to 2 indicates bi-excitonic emission, while a slope less than one confirms emission from localized excitons (in figure 1(e) the orange-shaded area) [27]. For our source the slope is $\alpha = 0.46$ confirming the presence of a defect. Finally, the photostability of the emission is investigated by continuously exciting the defect D1 and recording the single photon count rate. Figure 1(f) shows an average count rate of $\overline{R}_{\mathrm{PL}} = 3.09 \times 10^6 \ \mathrm{s}^{-1}$ and a standard deviation of $\sigma_{\mathrm{PL}} = 40.1 \times 10^3 \ \mathrm{s}^{-1}$. The fluctuations follow an expected Poisson distribution. We intensity-stabilized the laser diode such that the fluctuations of the laser are small compared to the fluctuations of the single photon count rate. The devices are stable for at least > 4 months if stored at room temperature and normal pressure as the first device fabricated is still operational and we could not find a significant change (less than 7%) in single photon count rate or correlation function (see below). This proves that the source is able to operate on long timescales also under field conditions and paves the way for integration into future experiments.

2.3. Correlation function measurements

In order to confirm the true quantum nature of the emitted photons the second-order correlation function is measured using a Hanbury Brown and Twiss-type (HBT) interferometer with the

setup used as shown in figure 2(a). A laser beam is split into a pump beam and a reference beam which is utilized for alignments. The pump beam is expanded and then coupled into a home-built confocal microscope, with the fiber-end with the defect loaded at the diffraction-limited focal spot of a microscope objective (Olympus MPlanFL N 50*x*/0.8). The setup only utilizes off-the-shelf components and a standard laser diode. Other than in the usual in-reflection geometry, where the excitation and collection of the emission is done via the objective, here, in a first experiment the defect is excited via the objective, but the emission is directly collected with the fiber. Then, at the other end of the fiber, the light is collimated and possible remains of the pump light are filtered out. The light is then split by a 50:50 beam splitter and finally detected by two SPADs (PerkinElmer SPCM-AQR-16). The special feature of this experiment is that the photons can be generated in the same setup into the fiber or into free space, just by flipping four mirrors and re-positioning the longpass filter used to filter out the pump light (see figure 2(b)). Thus, this setup offers to switch easily between free space single photon generation and fiber-coupled single photon generation. Note that the reference beam (see above) is also coupled into the HBT interferometer which then automatically couples the free space emission into the detectors. The results for fiber-coupled and free space operation are shown in figures 2(c) and (d), respectively. The second order correlation function can be described with

J. Phys. D: Appl. Phys. 50 (2017) 295101

T Vogl et al

$$g^{(2)}(\tau) = 1 - A_1 \exp\left(-\left|\frac{\tau - \mu}{t_1}\right|\right) + A_2 \exp\left(-\left|\frac{\tau - \mu}{t_2}\right|\right) \quad (3)$$

with A_1 and A_2 being the antibunching and bunching amplitude respectively and t_1 and t_2 being the characteristic antibunching and bunching time respectively. The parameter μ corrects for slightly different optical and electrical path lengths in the HBT interferometer. Also $g^{(2)}(\tau)$ has been normalized such that $g^{(2)}(\tau) \to 1$ for $\tau \to \infty$. From the fit we extract a $g^{(2)}(0) = 0.18 \pm 0.04$ for fiber-coupled operation and a $g^{(2)}(0) = 0.34 \pm 0.03$ for free space operation clearly indicating that the source is operating in the single photon regime. The differences in the $g^{(2)}$ for free space and fiber-coupled operation can be explained by the fact that it is harder to address the distinct defect while pumping through the back end of the fiber and performing a free space readout.

2.4. Collection efficiency

We now turn to a calculation of the collection efficiency for the fiber. Contrary to an NV-center embedded in the high refractive index material of bulk diamond, this source has an intrinsic out-coupling efficiency of unity as no total internal reflection is restricting the efficiency to collect the emission. While the emission is often assumed to be isotropic into 4π, polarization-resolved PL from quantum emitters showed that the emitters typically exhibit an in-plane dipole [5, 10]. For an ideal dipole oriented perpendicular to the collection direction the fraction of the collected photons η_ϕ by an optical component with an acceptance angle $\phi = 2\sin^{-1}(NA)$ (full angle) is calculated using antenna theory:

$$\eta_\phi = T_0 \cdot (T_1 + T_2 \cdot T_3) \quad (4)$$

where

$$T_0 = \frac{\phi}{2\pi} \quad (5)$$

$$T_1 = \frac{1}{2\pi}(2\phi - \sin(2\phi)) \quad (6)$$

$$T_2 = \frac{4}{\pi}\sqrt{\cos^{-2}(\phi/2) - 1} \quad (7)$$

$$T_3 = \left(1 + \tan^2(\phi/2)\sqrt{\cos^{-2}(\phi/2) - 1}\right)^{-2}. \quad (8)$$

The distance between collection optics and emitter is assumed to be small compared to the diameter of the optics. For a numerical aperture $NA = 0.5$ we find a collection efficiency of $\eta_\phi = 10.15\%$. Note that with this configuration the fiber has overfilled launch conditions making it sensitive to bending loss.

3. Conclusion

Aside from the measurements carried out with the TRPL setup the defect was excited with a laser in continuous wave

mode. This yields of course single photons in continuous wave mode which are not useful for quantum information processing. Using a short-pulsed excitation laser will allow testing the single photon source in a real quantum information experiment. In order to maintain the compactness of the single photon source a short-pulsed vertical-cavity surface-emitting laser (VCSEL) can be utilized. It is also possible to transfer the hBN onto the input port of a waveguide chip which would include the source directly on chip. We note that the difficulty of transferring onto a waveguide is the same as transferring onto a fiber.

In future experiments we will also test other materials and other specific defect types as well as different sample thicknesses and defect activation methods as it is then possible to achieve a narrower spectrum this way [10]. The defect then can be placed in between two distributed Bragg reflectors (DBRs), which suppresses noise and thus improves the $g^{(2)}(\tau = 0)$, enhances the directionality of the emission and cleans the spectrum.

In conclusion, we fabricated a fiber-integrated single photon source in few-layered hBN. The emitted single photons can be collected via free space- or fiber-coupled-mode just by switching the pump direction. Our setup shows the versatility of the source, as it is operational at room temperature. Measurements of the second-order correlation function dipping below 0.5 indicates that the source is operating in the quantum regime. Although these results are already promising, improvements suggested above making use of advantages of having the emitter in a cavity will improve the single photon properties. This will then pave the way for high quality single photon quantum information experiments with integrated photonics.

Note added: While preparing this manuscript we became aware of a recent similar work from the groups of Aharonovich and Takeuchi [28].

References

[1] Butler S Z et al 2013 ACS Nano **7** 2898
[2] Gupta A, Sakthivel T and Seal S 2015 Prog. Mater. Sci. **73** 44
[3] Geim A K and Novoselov K S 2007 Nat. Mater. **6** 183
[4] Novoselov K S, Fal'ko V I, Colombo L, Gellert P R, Schwab M G and Kim K 2012 Nature **490** 192
[5] Tonndorf P et al 2015 Optica **2** 347
[6] Srivastava A, Sidler M, Allain A V, Lembke D S, Kis A and Imamoğlu A 2015 Nat. Nanotechnol. **10** 491
[7] He Y M et al 2015 Nat. Nanotechnol. **10** 497

J. Phys. D: Appl. Phys. **50** (2017) 295101

T Vogl *et al*

[8] Koperski M, Nogajewski K, Arora A, Cherkez V, Mallet P, Veuillen J Y, Marcus J, Kossacki P and Potemski M 2015 *Nat. Nanotechnol.* **10** 503

[9] Chakraborty C, Kinnischtzke L, Goodfellow K M, Beams R and Vamivakas A N 2015 *Nat. Nanotechnol.* **10** 507

[10] Tran T T, Bray K, Ford M J, Toth M and Aharonovich I 2016 *Nat. Nanotechnol.* **11** 37

[11] Kok P, Munro W J, Nemoto K, Ralph T C, Dowling J P and Milburn G J 2007 *Rev. Mod. Phys.* **79** 135

[12] Gisin N, Ribordy G, Tittel W and Zbinden H 2002 *Rev. Mod. Phys.* **74** 145

[13] Ma X, Yuan X, Cau Z, Qi B and Zhang Z 2016 *NPJ Quantum Inf.* **2** 16021

[14] Fedrizzi A, Herbst T, Poppe A, Jennewein T and Zeilinger A 2007 *Opt. Express* **15** 15377

[15] Wang Q *et al* 2008 *Phys. Rev. Lett.* **100** 090501

[16] Zhong T, Hu X, Wong F N C, Berggren K K, Roberts T D and Battle P 2010 *Opt. Lett.* **35** 1392

[17] Wang X L *et al* 2016 *Phys. Rev. Lett.* **117** 210502

[18] Rambach M, Nikolova A, Weinhold T J and White A G 2016 *APL Photon.* **1** 096101

[19] Heinze D, Breddermann D, Zrenner A and Schumacher S 2015 *Nat. Commun.* **6** 8473

[20] Ding X *et al* 2016 *Phys. Rev. Lett.* **116** 020401

[21] Somaschi N *et al* 2016 *Nat. Photon.* **10** 340

[22] Daveau R S *et al* 2017 *Optica* **4** 178

[23] Babinec T M, Hausmann B J M, Khan M, Zhang Y, Maze J R, Hemmer P R and Lončar M 2010 *Nat. Nanotechnol.* **5** 195

[24] Gorbachev R V *et al* 2011 *Small* **7** 465

[25] Nam C W and Ashok S 1995 *Proc. ICSICT* 4 565

[26] Singh S P, Gangwar R and Singh N 2007 *Prog. Electromagn. Res.* **74** 379

[27] Miyauchi Y, Iwamura M, Mouri S, Kawazoe T, Ohtsu M and Matsuda K 2013 *Nat. Photon.* **7** 715

[28] Schell A W, Takashima H, Tran T T, Aharonovich I and Takeuchi S 2017 *ACS Photonics* **4** 761